Electrical properties of PZT aerogels

Stefan Geis[a], Jochen Fricke[a], Peer Löbmann[b],*

[a]*Physikalisches Institut der Universität Würzburg, Am Hubland, D-97074 Würzburg, Germany*
[b]*Fraunhofer-Institut für Silicatforschung, Neunerplatz 2, D-97082 Würzburg, Germany*

Abstract

PZT aerogels are prepared by sol-gel processing and subsequent supercritical drying. After sintering of the highly porous and uncalcined green body for up to 16 h in the temperature interval from 650 to 950 °C, a porous ceramic with a perovskitic PZT backbone is obtained. These PZT aerogels were characterized in terms of a possible application as ultrasound transducers. Samples were sintered in the temperature range between 650 and 950 °C and their elastic modulus was determined. Dielectric permittivities and dielectric charge constants were measured, the results can be interpreted with respect to the porosity and surface area of the samples. The electrical resistance of PZT aerogels is low compared to bulk material, a significant contribution of surface layer conductivity could be determined. The resulting low electrical breakdown field strengths hinder polarization. Additionally the inhomogeneous distribution and small strength of local poling fields has to be considered. Nevertheless dielectric hysteresis loops were obtained for samples annealed at 850 and 950 °C, respectively. © 2002 Elsevier Science Ltd. All rights reserved.

Keywords: Aerogels; Dielectric properties; Electrical properties; Porosity; PZT; Sol-gel processes

1. Introduction

Conventional piezoelectric ceramics such as $Pb(Zr_{0.53}Ti_{0.47})O_3$ (PZT) are commonly used as ultrasonic transducers. Their acoustic impedance is close to the one of other dense and solid materials. However, medical imaging or sonar applications require ultrasound transmission into tissue or water, i.e. materials of lower density and thus also of lower impedance. In order to prevent acoustic mismatch between transducers and medium, composites of conventional PZT ceramics with a second phase of lower density were used. Therefore, porous PZT-ceramics have been developed by a conventional mixed-oxide process.[1] Even lower transducer impedances are required for ultrasonic applications in air, e.g. ranging. In this case acoustic impedance matching between dense PZT ceramics and air can be obtained by using a quarter wave silica aerogel coupling layer. This, however, is a narrow band solution, which may increase the transmitted sound energy by 20 dB for the selected frequency.[2,3]

A broadband solution requires impedance matching of the piezoelectric material itself. This idea triggered the development of porous piezoelectric aerogels with a crystalline PZT backbone. Before 1995 two attempts to produce piezoelectric aerogels have been reported.[4,5] Some of our more recent synthetic efforts regarding this topic have already been described[6] and patents have been issued.[7,8] It should be noted that PZT aerogels are monolithic materials with a crystalline backbone. In contrast to this, most aerogel compositions known from the literature are either amorphous or can only be prepared as crystalline powders. Carbon aerogels show a mixed composition, with graphitic microcrystallites embedded in amorphous phases.[9]

2. Sample preparation

The precursor solution for PZT gels is prepared according to a procedure based on a method previously reported by Philips et al.:[10] a mixture of Zr- and Ti-propoxides (molar ratio 53:47) is chelated with 1 mol acetylacetone per mol metal, before lead acetate trihydrate dissolved in 1,3-propanediol is added. A molar excess of 5% lead is included to compensate for losses

* Corresponding author. Tel.: +49-931-4100-404; fax: +49-931-4100-498.

E-mail address: loebmann@isc.fhg.de (P. Löbmann).

during annealing. After keeping the solution at 150 °C for 4 h the volatile components are distilled off at reduced pressure. The highly viscous residue is diluted in 1,3-propanediol to yield a 1.5 M precursor solution with respect to $Pb_{1.05}Zr_{0.53}Ti_{0.47}O_3$, as confirmed by chemical analysis.

Alcogels were prepared by hydrolysis with 15 mol H_2O per mol PZT in flat-bottomed glass-containers with diameters of 28 mm. In most cases, gelation occurred within 5 h. The samples were aged at 50 °C for 14 days, subsequently the liquid phase of the gel was exchanged by repeatedly immersing the samples in fresh isopropanol over a week.

Supercritical extraction of this solvent starting at $p = 120$ bar and $T = 260$ °C yielded monolithic aerogels with high Pb^0 content.[11]

Prior to sintering all aerogels were heated up with 1 K min^{-1} in air and held at 400 °C for 10 h. The final sintering at 650, 750, 850 and 950 °C was performed within closed Al_2O_3 crucibles using the same heating rates. Usually, 5 samples were sintered at each temperature for 0, 2, 4, 8 and 16 h. In order to minimize lead loss at higher temperatures, a mixture of PbO and $PbZrO_3$ was used within the sintering containers to provide a Pb saturated atmosphere.

Circular electrodes were fabricated by vacuum deposition of silver on the top and bottom surfaces of the aerogel disks.

Poling was performed in a bath of completely fluorinated carbon (FC 70, 3M) by applying 10^3 kV/m for 20 min.

3. Measurement techniques

3.1. Densities

The effective densities ρ of the aerogels were calculated from weight and volume. These results were confirmed by measurements on a GeoPyc envelope density analyzer (Micromeritics Corporation, Norcross, GA, USA). All skeletal densities ρ_{sk} measured by He-pycnometry (Ultra-pycnometer 1000, Quantachrome Corporation, Boynton Beach, Fl, USA) were found to be (7.8 ± 0.1) g/cm^3 for samples annealed at 650 °C or above. Porosities II, therefore, were calculated as $II = 1 - \rho_{bulk}/(7.8 \text{ g cm}^3)$.

3.2. Ultrasonic measurements

Two identical transducers were pressed onto the sample disk while their distance was measured (Millitast, Mahr). A high voltage pulse (300 V) excited one transducer and triggered an oscilloscope (Hewlett Packard, 54602 A) that monitored the signal of the second transducer. Time of flight of the ultrasonic pulse was determined with an accuracy of ± 5 ns, i.e. about 0.1% for

samples disks of usual dimensions. At the same time, the transducer thickness was measured to within 0.1%. The ultrasound velocity c was determined from the ratio of transducer distance and time of flight. The elastic modulus

$$Y = \rho c^2 \tag{1}$$

was calculated assuming force free sidewalls and a sufficient large ratio of sample dimension and sound wavelength.

3.3. Electric measurements

In order to derive the temperature dependent conductivity, a sample and Pt thermocouple were placed inside a temperature-controlled furnace (Nabatherm, Eurotherm RHT-502). Between 200 and 500 °C, four pole voltage–current measurements were performed in steps of five Kelvin after holding for 5 min, using a multimeter (Hewlett Packard 3457 A). Structural changes were checked by SEM micrographs taken before and after measurement.

The dielectric permittivity was obtained by impedance measurements (Hewlett Packard, 4284 A) at 1 kHz.

For the determination of the hysteresis, symmetrical high voltage cycles of given voltage amplitude at a fixed frequency of 5 Hz were applied to the sample by a suitably connected pair of high voltage generators (Knürr Heinzinger PNC 40.000 and HNCs 100.000). Current monitoring allowed for integration of the polarization after a division by the sample area.

The same set-up allowed for a determination of the field strength for current breakdown.

The charge constants d_{33} and d_{31} were measured with a custom-built piezometer system (Take Control Ltd.). An oscillating force (0.1 N rms, 300 Hz) was applied onto a given direction with respect to the poling axis. The periodic charge accumulation on the electrodes was detected via a shunted capacitance of 0.1 μF. The correct boundary condition for the measurement, i.e. open circuit conditions with $E = 0$ were assured by this capacitance that was orders of magnitude higher than the capacitance of the sample. Poling was performed 24 hours before the measurement.

4. Results and discussion

4.1. Elastic modulus

The elastic modulus Y is given in Fig. 1 in a double log plot as a function of absolute density ρ and relative density on the upper and lower x-axis, respectively. The parameter is the sintering temperature. The data for a Nd-doped bulk PZT ceramic (PXE52, Philips) are

included for comparison. Each data point is the average value from three identically prepared samples. A fit of the elastic moduli to the scaling law in Eq. (2) was performed on each series:

$$Y \propto (1\text{-}\Pi)^\alpha = \rho^\alpha \qquad (2)$$

The fit results are included in Fig. 1 as straight lines.

A strong increase of the elastic moduli in the range from 1 to 50 GPa with relative densities between 22 and almost 100% can be observed. As is indicated by the straight lines, all series can be described by a scaling behavior with an exponent close to $\alpha = 2$. As expected, the largest elastic moduli are obtained for the specimens sintered at 850 and 950 °C.

According to the scaling law theories of mechanical properties, an exponent $\alpha \approx 2$ like that observed that for the PZT aerogels indicates an efficiently connected backbone[12] in which a homogeneous elastic behavior of the whole backbone mass is observed. Exponents $\alpha > 2$ indicate a network with so called dead ends, i.e. parts of the backbone that do not participate in the elastic behavior.[13] Exponents $\alpha > 2$ are also observed if an inhomogeneous distribution of the mechanical load occurs, i.e. if the material consists of beads which are connected by small, mechanically inefficient necks.[14] Such a situation is typical for SiO_2 aerogels where $\alpha \approx 3.5$ are typical.[13]

4.2. Temperature dependent specific conductivity

The temperature dependent specific conductivity $\sigma(T)$ was measured on samples that were treated for 8 h at different sintering temperatures.

In Fig. 2, the results are given as function of the inverse absolute temperature in a semi logarithmic plot. The data for an Nd-doped and conventionally prepared dense PZT ceramic are included for comparison.[15]

In this presentation, a straight-line behavior is observed for the aerogels and for the bulk Nd-doped reference ceramic. Both materials have a similar slope. However, the PZT Aerogels have considerable larger conductivities especially the ones sintered at low temperatures.

The general temperature dependence of the conductivity is typical for a thermodynamically activated conductivity where only one carrier species dominates in the corresponding temperature interval. This allows for data fitting according to Eq. (3):

$$\sigma(T) = \sigma_\infty \exp(-E_{\text{act}}/k_B T), \qquad (3)$$

where k_B and T are Boltzmann's constant and the absolute temperature, respectively. The extrapolated conductivity σ_∞ is proportional to the charge carrier concentration n and mobility μ. These charge carriers have to overcome the activation energy E_{act} in order to participate in the current.

The σ_∞-values for the PZT aerogels are displayed on the left y-axis of Fig. 3 as a function of porosity. The ratio of relative density and grain size $(1-\Pi)/d_{\text{gs}}$ is displayed on the right y-axis.

All aerogels exhibit comparatively high σ_∞-values that increase with porosity in the range of 10–150 kS/m. The characteristic of the $(1-\Pi)/d_{\text{gs}}$-variation correlates with the one for the σ_∞ data except for the data at lowest porosity.
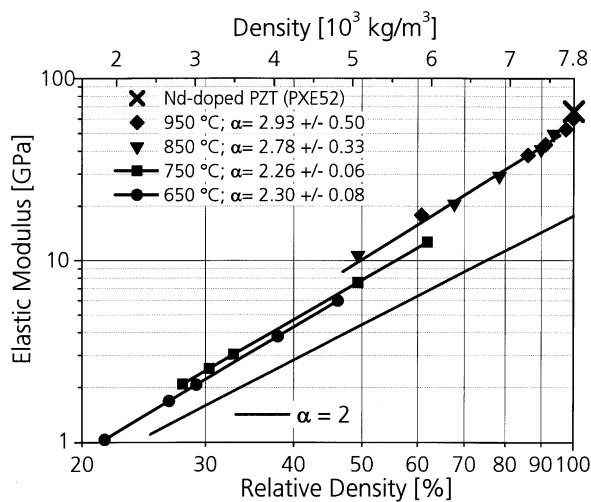

Fig. 1. Double log plot of the elastic modulus of PZT aerogels as a function of density for different sintering temperatures and the scaling exponents α for a fit according to the scaling law. The data for an Nd-doped dense ceramic (PXE52, Philips) and a calculated curve according to a scaling law with $\alpha = 2$ are included for comparison.
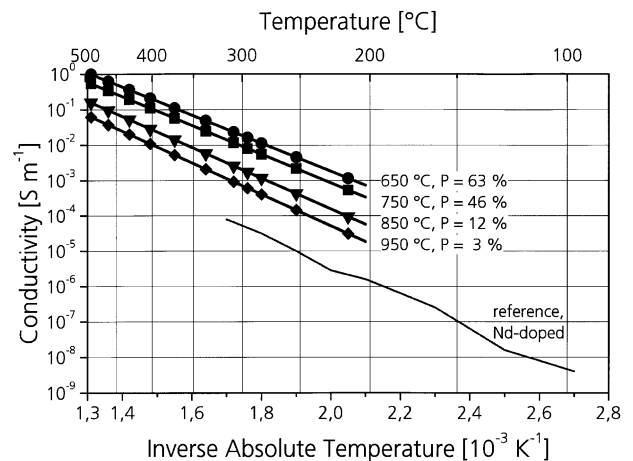

Fig. 2. The temperature dependent specific conductivity is given as function of the inverse absolute temperature and temperature in °C and on the upper and lower x-axis, respectively. Parameters are the sintering temperature and porosity. Data of an Nd-doped reference is included.[15]

The depicted σ_∞-values are considerably higher than for the Nd-doped bulk PZT ceramic. Accordingly, charge transport cannot be explained in terms of a bulk PZT property.

It can be shown, that the volume specific surface area of an aerogel is proportional to the $(1-\Pi)/d_{gs}$-ratio if the aerogel density consists of hard spheres with bulk PZT density and grain size d_{gs} as diameter.

The behavior in Fig. 3 thus, is indicative for electrical conduction along the inner surface of the porous body in addition to the conduction within the PZT bulk backbone. This additional surface current is assumed within a constant given thickness of 0.1–0.01 μm.[16]

It can be suggested, that the high concentration of charge carriers in the surface layer is due to the specific PZT aerogel processing. During the sinter process, the inner surface is in contact with the atmosphere and, thus, is prone to chemical interaction with the gaseous environment. A high amount of impurities, defects and vacancies can be accumulated there upon sintering.

In addition to the conductivity σ_∞, also the activation energy E_{act} can be derived. E_{act} increases with decreasing porosity from 0.91 eV down to 0.82 eV. A comparable value for E_{act} of 0.82 eV is found for the Nd doped reference.

Conduction across the inner surface causes current breakdown upon poling and thus limits the applicable field strengths.

4.3. Dielectric permittivity

Like in the case of the elastic modulus, the dielectric permittivity ε was determined for a series of samples that were sintered at different temperatures. For each combination of sintering time and temperature, a set of three identically prepared samples was investigated.

Fig. 4 gives the results of these measurements as a function of absolute and relative density. A fit according to a model of enclosed pores[17] is included for the series at 950 °C.
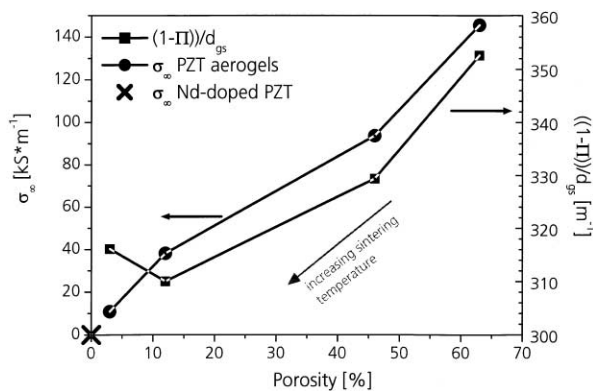
Fig. 3. The extrapolated conductivity σ_∞ (left ordinate) is given as a function of porosity. On the right ordinate, the ratio of relative density and grain size, i.e. $(1-\Pi)/d_{gs}$, is shown.

$$\varepsilon_{PZT aerogel} - 1 = (1 - \Pi)\varepsilon_{PZT}[1 + N_i \cdot \varepsilon_{PZT}] \qquad (4)$$

The depolarization factor N_i is analogous to the ferromagnetic case and depends linearly on porosity Π: $N_i = c_{dep} \cdot \Pi$. The proportionality factor c_{dep} is a measure for the effectivity of electric field shielding and decreases with pore size.

The dielectric permittivity increases first moderately than drastically with relative density. At all sintering temperatures, the dielectric permittivity of the aerogels increases not only as a direct consequence of decreasing porosity. In addition, a decreasing porosity is accompanied by an increase of the backbone permittivity that is especially strong for 850 and 950 °C sintering.

This cooperative influence of decreasing porosity and increasing backbone permittivity prohibits fitting of the whole permittivity data of the PZT aerogels according to a general mixing rule like:

$$\varepsilon_{aerogel} = \varepsilon_{PZT}\, f(P) \qquad (5)$$

The theory of Igarashi [Eq. (4)] fits the data for the time series at 950 °C optimally.[17] A dielectric permittivity for the bulk PZT phase of 490 and a comparatively large proportionality factor of 0.03 between porosity and depolarization was obtained. These values keep the χ^2-test below 10^{-2}.

4.4. Ferroelectric properties

The plot in Fig. 5 compares the hysteresis curves for PZT aerogels of 17 and 25% porosity with the one of a dense and Nd-doped PZT ceramic (PXE52, Philips) on the left and right y-axis.
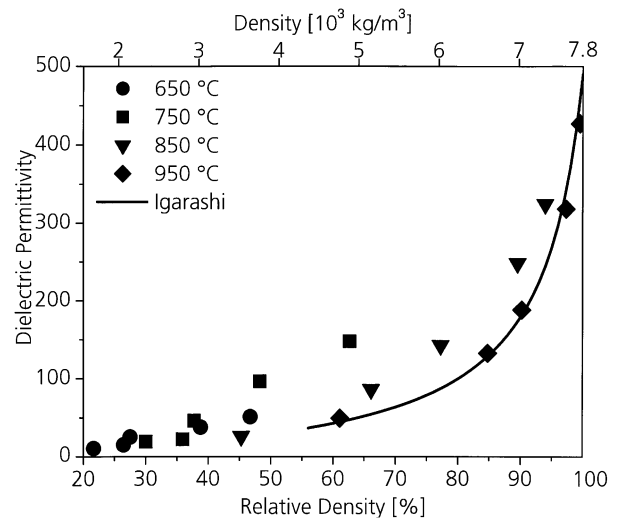
Fig. 4. The variation of the dielectric permittivity of PZT aerogels with relative density. Parameter is the sintering temperature. The fit curve was derived for the 950 °C samples according to Eq. (4).
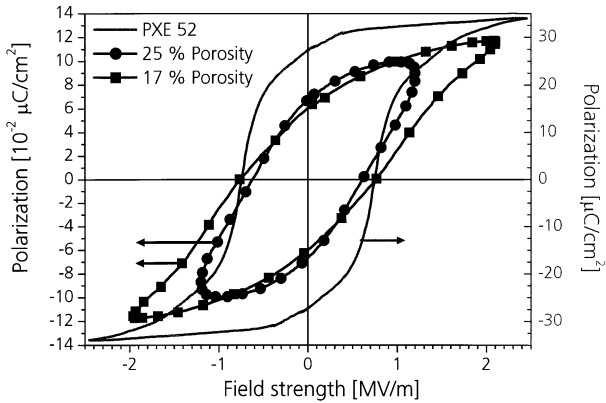
Fig. 5. Polarization versus electrical field for two PZT aerogels (on the left y-axis) and a Nd-doped dense PZT ceramic (on the right y-axis).

At a coercive field E_c of 0.7 MV/m, the polarization of the Nd-doped ceramic increases from zero with a high slope. The slope is almost zero at the maximal field where the saturated polarization P_s is reached. Then, the polarization decreases linearly as the field is reduced from its peak value. This is followed by a non-linear decrease that crosses the remanent polarization P_r at zero field and reaches zero polarization for $E = -E_c$.

In contrast, the hysteresis loops of both PZT aerogels are more ellipsoidal. For the shown cases, the polarization varies non-linearly throughout the whole hysteresis cycle. While the E_c-values are similar to the PXE52 case, the variation of the polarization around the corresponding E_c values is considerably weaker than for the dense bulk PZT ceramic. P_r of the PZT aerogels is only about $6 \cdot 10^{-2}$ μC/cm^2, while $P_s \approx (10–11) \cdot 10^{-2}$ μC/cm^2.

An explanation of these observations can be given by the following: Porosity implies an inhomogeneous distribution of the local (poling) fields. The electric field distribution curve in Ref. 18 shows, that an external electric field is transformed into a distribution of local fields around a reduced mean value. Hence, different domains or grains switch at different values of the external field. An increase in porosity is accompanied by a broader distribution of the local fields. As a result, consecutive domain switching causes a decreasing slope and a smoother variation of the polarization during the whole hysteresis cycle. At the same time, an increasing porosity shifts the external field strength to smaller local fields. Hence, a porous ferroelectric material has a reduced polarization compared to a similar but dense material if both are poled with identical external field strengths. This is shown for a mixed oxide processed PZT[19] with 52% porosity, which has a remanent polarization of 3 μC/cm^2 compared to 30 μC/cm^2 for the Nd-doped and dense PZT reference.

The investigated PZT aerogels exhibit an additional reduced polarization compared to the above porous PZT. Here, a low degree of crystallinity is accompanied by an additional reduced amount of ferroelectric domains. In addition, a partial shielding of electric fields

by a conductive surface layer reduces the amount of polarized grains as a shielded grain requires higher electric fields to be poled or remains unpolarized.

Fig. 6 gives the coercive E_c and breakdown E_{deg} fields as a function of porosity for two aerogel series obtained from sintering at 850 and 950 °C.

Coercive and breakdown fields decrease with porosity as can be expected. The ratio of breakdown and coercive field is only around two in each case, which is the reason for the small polarization.

4.5. Charge constants d$_{33}$ and -d$_{31}$

The piezoelectric charge constants d_{33} and $-d_{31}$ are a measure for the electric charge density that is generated by a strain applied along a given axis to the previous poling direction. Accordingly, these constants depend on the amount of polarized piezoelectric material. By convention, the poling axis is the '3' axis, i.e. d_{31} measures the charge density in direction of the poling axis for an orthogonal stress. A piezoelectric ceramic with a high poling degree and a low porosity has large absolute values of the charge constants d_{33} and d_{31}.

Values for the piezoelectric charge constants d_{33} and $-d_{31}$ are given in Fig. 7 as a function of porosity for two different sintering temperatures. For simplicity, the negative values of d$_{31}$ are plotted and discussed in the following. Each data point is the average of two identically prepared samples that were sintered for 2, 4 or 8 h at 850 or 950 °C, respectively. Accordingly, the error bars correspond to the mean deviation from the average and are below 15% in each case.

All obtained values decrease with porosity. The highest charge constants d$_{33}$ are derived for the 950 °C specimens. After a 950 °C sintering for 2 h lower -d$_{31}$ values were obtained compared to a 850 °C sintering for 8 h
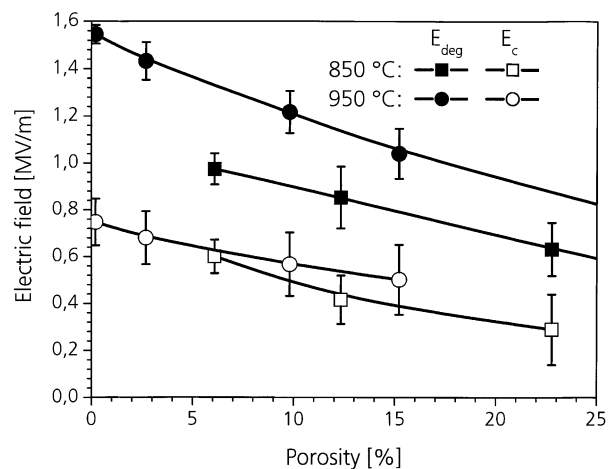

Fig. 6. Variation of the coercive (E_c) and breakdown (E_{deg}) fields as a function of porosity for two different sintering temperatures. A decreasing porosity corresponds to an increase in sintering time for each curve.
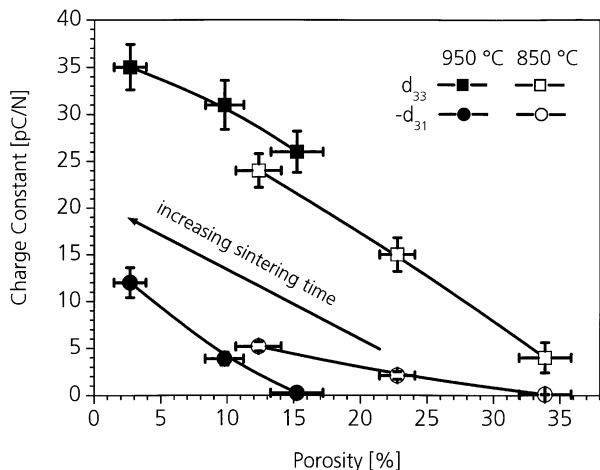
Fig. 7. Variation of the charge constants d_{33} and $-d_{31}$ with porosity for 850 and 950 °C. A decrease in porosity corresponds to an increasing sintering time for each curve.

even though the attained porosity is around 13% in both cases.

For PZT aerogels of increasing porosity, a reduced amount of piezoelectric material is available for the electro-mechanical coupling and lower charge constants are derived. Additional contributions to this decrease of the charge constants are the porosity dependence of the poling degree and of the specific conductivity. For example, high charge accumulations are prohibited by an increasing specific conductivity that lowers d_{33} and d_{31} likewise.

In the particular case of $-d_{31}$, strain is applied orthogonal to the poling direction. For a high $-d_{31}$, a strong coupling of parallel to orthogonal mechanical excitations is measured by the Poisson's ratio. For piezoelectric materials, the Poisson's ratio is expected to decrease with porosity.[20]

Accordingly, a higher $-d_{31}$-value after a 850 °C/8 h treatment compared to a 950 °C/2 h treatment to a similar porosity can be explained by a higher Poisson's ratio for the samples treated for a longer time at 850 °C. Even though the samples treated at 950 °C for 2 h are poled to a higher degree as the comparatively higher d_{33} values indicate, a smaller Poisson's ratio is responsible for the lower $-d_{31}$ values compared to the samples treated at 850 °C for 8 h.

Finally, it is worth mentioning, that no significant variation in the charge constants d_{33} and d_{31} could be found after prolonged exposure to the poling field. Accordingly, it can be concluded, that an increase of the poling time does not alter the poling degree.

5. Conclusions

This work showed, that the obtained monolithic, porous and crystalline PZT aerogels are porous ferro-electric—and, therefore, piezoelectric materials. The values derived for the hydrostatic charge constants at low porosities match the values of other PZT materials. PZT aerogels can be promising materials for passive sound detectors. Furthermore, they exhibit scaling exponents of the elastic modulus as a function of density that are close to two. This indicates efficient connectivity of the backbone and a homogeneous elastic behavior.

However, there is still room for improvement in terms of the microstructure (e.g. reduction of microcracks), lowering the conductivity and increase in the poling degree. Here, disadvantageous features like the poor mechanical stability or the high specific conductivity can be ascribed—at least indirectly—to the particular sinter process for the PZT Aerogels. This process starts with an open porous and uncalcined green body. In contrast to other porous PZT ceramics,[19,21,22] sintering and calcination cannot be separated for PZT Aerogels and both are performed with direct access of the sintering atmosphere to the open porous backbone. An indirect cause of this sintering strategy is the poor dielectric behavior in terms of conductivity and current breakdown. Low breakdown field strengths prohibit the application of high poling fields. Accordingly, the comparatively poor poling degree leads to small piezoelectric constants. Possible improvements of the PZT aerogels and novel production steps are currently investigated as infiltration of liquid sol into a wet gel. This results in a density gradient that can enhance impedance matching.

An improved microstructure can enable high temperature poling to achieve an increased poling degree. In this case, a sensor of high sensitivity would be feasible considering the comparable hydrostatic charge constants achieved at a low poling degree and for low porosities.

References

1. Galassi, G., Roncari, E., Craciun, F., Bettucci, A., Farrelly, F. and Alippi, A., Porous piezoelectric ceramics with high piezoelectric constants and very low acoustic impedance. In *Fourth Euro Ceramics*, Vol. 5, ed. G. Gusmano and E. W. Traversa. Gruppo Editoriale Faenza Editrice S.p.A., 1995, p. 25.

2. Gerlach, R., Kraus, O., Fricke, J., Eccardt, P., Kroemer, N. and Magori, V., Modified SiO$_2$ aerogels as acoustic impedande matching layers in ultrasound devices. *J. Non-Cryst. Solids*, 1992, **145**, 227.

3. Gerlach, R., Fricke, J. and Magori, V., German Patent Int. Cl. H 04 R 17/00 (1994); Gerlach, R., Fricke, J., Magori, V. Eur. Patent Int. Cl. CO1B 33/158 (1994).

4. Gaucher, P., Ganne, J., and Dubois, J., Eur. Patent Application 0 470 898 A1 02.08.1991.

5. Pethybridge, G., Dobson, P. and Brook, R., Aerogels. *Br. Ceram. Proc.*, 1994, **53**, 73.

6. Löbmann, P., Glaubitt, W., Geis, S. and Fricke, J., Development of ferroelectric aerogels. *J. Sol–Gel Sci. Technol*, 1999, **16**, 173.

7. Löbmann, P., Glaubitt, W. and Fricke, J., Eur. Patent Int.Cl. CO4B 35/491 (1997).

8. Löbmann, P., Glaubitt, W. and Fricke, J., US Patent Int.Cl. CO4B 35/49 (1999).

9. Petricevic, R., Pröbstle, H. Fricke, J., Chemical vapor infiltration of carbon into carbon aerogels. *J. Electrochem. Soc. Proc.*, in press.

10. Phillips, N., Calzada, M. and Milne, S., Sol-gel-derived lead titanate films. *J. Non-Cryst. Solids*, 1992, **147 and 148**, 285.

11. Löbmann, P., Glaubitt, W., Müller, G., Geis, S. and Fricke, J., Preparation of monolithic crystalline lead titanate aerogels. *J. Mater. Sci.*, 1998, **33**, 2371.

12. Groβ, J. and Fricke, J., Scaling of elastic properties in highly porous nanostructured aerogels. *NanoStruct. Mater.*, 1995, **6**, 905.

13. Groβ, J. and Fricke, J., Ultrasonic velocity measurements in silica, carbon and organic aerogels. *J. Non-Cryst. Solids*, 1992, **145**, 217.

14. Ma, H., Ma, H., Prevost, J., Jullien, R. and Scherer, G. W., Computer simulation of mechanical structure-property relationship of aerogels. Conference Proceedings of ISA 6, 2000. *J. Non-Cryst. Solids*, in press.

15. Gurevich, V. M., Electric Conductivity of Ferroelectrics. *Committee of Standards, Measures and Measuring Instruments of the USSR 1*, 1969. Translated from Russian by the Israel Program for Scientific Translation, Jerusalem, 1971, pp. 144.

16. Känzig, W., Space charge layer near the surface of a ferroelectric. *Phys. Rev.*, 1955, **98**(2), 549.

17. Igarashi, H., Tashoro, S. and Okazaki, K., Depolarization factor of dielectric ceramics including pores. *Mem. Def. Acad. Jpn.*, 1979, **19**, 87.

18. Getman, I. and Lopatin, S., Theoretical and experimental investigation on porous PZT ceramics. *Ferroelectrics*, 1996, **186**, 301.

19. Nagata, K., Igarashi, H. and Okazaki, K., Properties of an interconnected porous lead zirconate titanate $(Pb(Zr,Ti)O_3)$ ceramic. *Jap. J. Appl. Phys.*, 1980, **19**, 87.

20. Wersing, W., Lubitz, K. and Mohaupt, J., Dielectric, elastic and piezoelectric properties of porous PZT aerogels. *Ferroelectrics*, 1986, **68**, 77.

21. Hikita, K., Yamada, K., Nishioka, M. and Ono, M., Piezoelectric properties of the porous PZT and the porous PZT composite with silicone rubber. *Ferroelectrics*, 1983, **49**, 265.

22. Safari, A., Sagong, G., Giniewicz, J. and Newnham, R., Composite piezoelectric transducers. *Proceedings of the 21st University Conference on Ceramic Science*, 1986, **20**, 445.